NEURAL REGENERATION RESEARCH
www.nrronline.org

Research Article

Potential application of let-7a antagomir in injured peripheral nerve regeneration

Qian-Qian Chen[1, 2] Qian-Yan Liu[2], Pan Wang[2], Tian-Mei Qian[2], Xing-Hui Wang[2], Sheng Yi[2], Shi-Ying Li[2, *]

https://doi.org/10.4103/1673-5374.357914
Date of submission: April 27, 2022
Date of decision: July 26, 2022
Date of acceptance: August 23, 2022
Date of web publication: October 13, 2022

From the Contents

Graphical Abstract

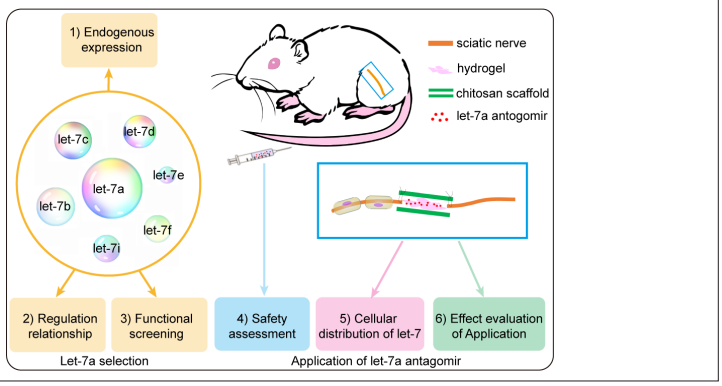

Abstract

Neurotrophic factors, particularly nerve growth factor, enhance neuronal regeneration. However, the *in vivo* applications of nerve growth factor are largely limited by its intrinsic disadvantages, such as its short biological half-life, its contribution to pain response, and its inability to cross the blood-brain barrier. Considering that let-7 (human miRNA) targets and regulates nerve growth factor, and that let-7 is a core regulator in peripheral nerve regeneration, we evaluated the possibilities of let-7 application in nerve repair. In this study, anti-let-7a was identified as the most suitable let-7 family molecule by analyses of endogenous expression and regulatory relationship, and functional screening. Let-7a antagomir demonstrated biosafety based on the results of *in vivo* safety assessments and it entered into the main cell types of the sciatic nerve, including Schwann cells, fibroblasts and macrophages. Use of hydrogel effectively achieved controlled, localized, and sustained delivery of let-7a antagomir. Finally, let-7a antagomir was integrated into chitosan conduit to construct a chitosan-hydrogel scaffold tissue-engineered nerve graft, which promoted nerve regeneration and functional recovery in a rat model of sciatic nerve transection. Our study provides an experimental basis for potential *in vivo* application of let-7a.

Key Words: chitosan; chitosan-hydrogel scaffold; let-7; let-7a antagomir; miRNA; nerve graft; peripheral nerve injury; peripheral nerve regeneration; Schwann cells

Introduction

Peripheral nerve injury is a common clinical problem that affects approximately 13–23 per 100,000 persons per year (Li et al., 2014; Lolis et al., 2018). Currently, the gold standard treatment for peripheral nerve injury is autologous nerve grafting. The application of autologous nerve grafts, however, is largely limited by its intrinsic disadvantages, such as limited donor nerve sources, donor nerve functional loss, and size differences between the donor nerve and recipient nerve (Gu et al., 2011; Luo et al., 2021). Therefore, there is an urgent need to develop and construct tissue-engineered nerve grafts with better clinical application to repair injured peripheral nerves.

Tissue-engineered nerve grafts have been designed as a prospective alternative for regenerative medicine. Tissue-engineered nerve grafts generally contain scaffolds and embedded supporting cells or biological cues. Morphological and cellular molecular studies have demonstrated that axonal regeneration involves the precise coordination of numerous cells to provide an optimal regeneration microenvironment (Wang et al., 2022a). Macrophages, fibroblasts, and Schwann cells gather at the injury site to perform different functions and help establish a regenerative pathway to repair peripheral nerve function (Qian et al., 2018; Wang et al., 2022a). Many growth factors with neurotrophic effects, especially nerve growth factor (NGF), promote myelin sheath formation, enhance axonal regeneration, and have been used in neural tissue engineering (Gu et al., 2011, 2014). However, the *in vivo* applications of these growth factors are largely restricted by their low stability, short half-life periods, and high costs (Chen and Mooney, 2003; Chen et al., 2012). Recent studies have reported that a variety of microRNAs (miRNAs) regulate peripheral nerve injury and regeneration (Li et al., 2015b; Ji et al., 2019; Lopez-Leal et al., 2020; Wang et al., 2022c). Therefore, it is feasible to incorporate miRNAs into biomaterial scaffolds to reshape the microenvironment, so as to promote injured nerve regeneration (Krutzfeldt et al., 2005; Gu et al., 2014; Yu et al., 2015; Ou et al., 2019; Leng et al., 2020). Many reviews have discussed the possibilities of various miRNA applications, especially the therapeutic application of miRNA for tissue engineering (Hutchison et al., 2013; Zhao et al., 2014; Caputo et al., 2015; Chew, 2015; Li et al., 2015a; Miller et al., 2015; Raschzok et al., 2015; Sabirzhanov et al., 2016; Yao et al., 2016).

Let-7, the first identified human miRNA, is involved in many important biological processes (Shell et al., 2007; Roush and Slack, 2008; Su et al., 2012; Yuan et al., 2012). Previous studies showed that decreased let-7 levels elevated NGF secretion from Schwann cells, increased Schwann cell proliferation and migration *in vitro*, and promoted Schwann cell migration and axon outgrowth *in vivo* (Li et al., 2015b; Zhang et al., 2020). Another study showed that let-7 miRNAs were core regulators affecting peripheral nerve repair and regeneration (Wang et al., 2019). Considering these studies, we selected let-7a as a suitable member of the let-7 family, performed a safety assessment for potential application, and investigated its morphological and functional effects on peripheral nerve injury repair.

[1]State Key Laboratory of Pharmaceutical Biotechnology and Ministry of Education Key Laboratory of Model Animal for Disease Study, Model Animal Research Center, Medical School, Nanjing University, Nanjing, Jiangsu Province, China; [2]NMPA Key Laboratory for Research and Evaluation of Tissue Engineering Technology Products, Key Laboratory of Neuroregeneration of Jiangsu and Ministry of Education, Co-innovation Center of Neuroregeneration, Nantong University, Nantong, Jiangsu Province, China
*Correspondence to: Shi-Ying Li, PhD, lisy0379@ntu.edu.cn.
http://orcid.org/0000-0001-5150-7299 (Shi-Ying Li)

Funding: *This work was supported by the National Natural Science Foundation of China, No. 31970968 (to SYL), the Collegiate Natural Science Foundation of Jiangsu Province, No.16KJA310005 (to SYL), Priority Academic Program Development of Jiangsu Higher Education Institutions [PAPD] and the Natural Science Foundation of Jiangsu Province, No. BK20200976 (to XHW).*
How to cite this article: *Chen QQ, Liu QY, Wang P, Qian TM, Wang XH, Yi S, Li SY (2023) Potential application of let-7a antagomir in injured peripheral nerve regeneration. Neural Regen Res 18(7):1584-1590.*

Methods

Animals and ethics statement

Specific-pathogen-free grade neonatal 1-day-old Sprague-Dawley (SD) rats and healthy adult male SD rats (8 weeks old, 180–220 g) were purchased from the Animal Experimental Center of Nantong University, Jiangsu, China (license No. SYXK (Su) 2017-0046) and housed with free access to food and water (five rats per cage) in a standard facility with constant temperature (18–26°C) and humidity. Experimental procedures were conducted in accordance with Institutional Animal Care guidelines of Nantong University and were ethically approved by Administration Committee of Experimental Animals Jiangsu, China (approval No. 20180301-009) on March 3, 2018. The study design and timeline are shown in **Additional Figure 1**.

Cell culture and transfection

Neonatal 1-day-old SD rats were anesthetized and then sacrificed by decapitation, after which primary Schwann cells were collected from sciatic nerve stumps and digested with collagenase type I (Cat# C0130, Sigma, St. Louis, MO, USA) followed by trypsin (Cat# 25300, Thermo Fisher Scientific, Waltham, MA, USA). The cells were cultured in cell complete medium containing 4.5 g/L glucose Dulbecco's Modified Eagle Medium (DMEM; Cat# 10-013, Corning, Steuben County, NY, USA) with 10% fetal bovine serum (FBS; Cat# 10099141c, Gibco, Carlsbad, CA, USA) for 12 hours. Schwann cells were gently suspended from the dish by a pipette, cultured and further purified with anti-Thy1.1 antibody (1:1000, Cat# M7898, Sigma) and rabbit complement (Cat# 310203, Invitrogen, Carlsbad, CA, USA), as previously described (Li et al., 2015b). Fibroblasts remaining on the bottom of the dish were directly cultured in DMEM with 10% FBS. Macrophages (RAW264.7, National Collection of Authenticated Cell Cultures, Shanghai, China) were cultured in DMEM containing 10% FBS and 1% L-glutamine (Cat# 25030149, Gibco). All cells were cultured in an incubator at 37°C with 5% CO_2. Immunofluorescence was used to determine the purity.

Cultured cells were transfected with 20 nM let-7 mimic (let-7 *in vitro*), 100 nM let-7 inhibitor (anti-let-7 *in vitro*), and the corresponding mimic or inhibitor control (RiboBio, Guangzhou, Guangdong Province, China) using Lipofectamine RNAiMAX transfection reagent (Invitrogen) following the manufacturer's instructions.

Quantitative RT-PCR

Total RNA was isolated from cultured Schwann cells using RNA-Quick Purification Kit (Esunbio, Shanghai, China) and reverse transcribed using TaqMan MicroRNA Reverse Transcription Kit (Applied Biosystems, Foster City, CA, USA). Quantitative reverse transcription polymerase chain reaction (RT-PCR) was performed using QuantiNova SYBR Green PCR Kit (Qiagen, Hilden, Germany) on a Stepone real-time PCR System (Applied Biosystems). The primers for reverse transcription and PCR were from the Bulge-loop™ miRNA qRT-PCR Primer Sets (Ribobio). The thermocycler program was as follows: 5 minutes at 95°C; 30 cycles of 15 seconds at 95°C, 30 seconds at 60°C; 15 seconds at 95°C; and 1 minute at 60°C. Relative expression levels of let-7 were normalized to U6 expression using the ΔCt method ($2^{-\Delta\Delta Ct}$) (Livak and Schmittgen, 2001).

EdU cell proliferation assay

Schwann cells were resuspended, seeded onto 96-well plates at a volume of 100 µL and a density of 2×10^5 cells/mL, and transfected with let-7 mimic, let-7 inhibitor, or the corresponding controls for 24 hours. Next, 100 µM 5-ethynyl-2′-deoxyuridine (EdU; RiboBio) was added to DMEM (Corning) with 10% FBS (Gibco), and cells were cultured for an additional 12 hours. After fixation with 4% paraformaldehyde, Schwann cell proliferation rate was measured with Cell-Light EdU DNA Cell Proliferation Kit (RiboBio), and nuclei were stained with Hoechst (RiboBio). Images were captured with a DMR fluorescence microscope (Leica Microsystems, Bensheim, Germany).

Transwell-based cell migration assay

Schwann cells transfected with let-7 mimic, let-7 inhibitor, or the corresponding controls were resuspended in DMEM (Corning) and seeded onto the upper chamber of a 6.5-mm transwell with 8-µm pores (Corning) at a volume of 100 µL and a density of 3×10^5 cells/mL. The bottom chamber of the transwell was filled with 500 µL cell complete culture medium as described above. After 24 hours of incubation, Schwann cells remaining on the upper surface of the upper chamber were cleaned with a cotton swab, and Schwann cells that migrated to the bottom surface were stained with 0.1% cresyl violet (Cat# C8470, Solarbio, Beijing, China). Images were captured with a Leica DMI3000 B (Leica Microsystems). Migrated cells were dissolved in cresyl violet with 33% acetic acid (Cat# 64-19-7, Xilong Scientific, Guangzhou, Guangdong Province, China) and the absorbance of cresyl violet staining was measured using a Synergy™ 2 Multi-Mode Microplate Reader (BioTek, Burlington, VT, USA).

Biosafety assessment

Twenty adult male SD rats (8 weeks old) were randomly divided into two groups (six rats in each group) and injected with 1 mL saline (negative control, Con) or 100 nmol let-7a antagomir (anti-let-7a *in vivo*, RiboBio) dissolved in 1 mL saline through caudal vein injection. At 5 days after injection, rats were anesthetized with mixed narcotics (42 mg/kg magnesium sulfate, 85 mg/kg trichloroacetaldehyde monohydrate, 17 mg/kg sodium pentobarbital; Sigma) and sacrificed. After transcardial perfusion with 0.9% normal saline followed by 4% paraformaldehyde (PFA; Xilong Scientific), the heart, liver, spleen, lung, and kidney were collected. The fixed tissues were embedded in paraffin, dehydrated by ethanol gradient, and then cut into 8-µm sections. Hematoxylin-eosin staining (Cat# C0105, Beyotime, Shanghai, China) was performed for histopathological examinations under an Axio Imager M2 microscope (Carl Zeiss Microscopy GmbH, Jena, Germany). At 5 days and 4 weeks after injection, blood samples were taken from the rats, and cellular and electrolyte parameters, biochemical parameters, and immunological parameters in the blood were measured.

Flow cytometry analysis and cellular immunofluorescence analysis

Eighteen adult rats were exposed and subjected to 3-mm sciatic nerve crush (Shen et al., 2022) with a forceps after anesthetization. Immediately after injury, 5 nmol let-7a antagomir was injected in each rat at the injury site. Flow cytometry was conducted to measure the proportions of Cy3-labeled let-7a antagomir-positive cells at 1 and 4 days (six rats at each time point) after nerve injury. Rat sciatic nerve stumps were harvested and trypsin-digested with 3 mg/mL collagenase type I for 3 hours, followed by 0.25% trypsin at 37°C for 1 hour. Then, the cells were filtered and fixed with 100 µL Fixed Kit (70-GAS003, MultiSciences, Hangzhou, Zhejiang, China) according to the manufacturer's instructions for 15 minutes. Cells were incubated with primary antibodies rabbit anti-S100β antibody (Schwann cell marker; 1:100, Cat# Ab52642, Abcam, Cambridge, MA), mouse anti-P4HB antibody (fibroblast marker; 1:100, Ab2792, Abcam), and mouse anti-CD68 antibody (macrophage marker; 1:200, Ab31630, Abcam) at room temperature for 1 hour followed by Alexa Fluor 488 donkey anti-rabbit IgG (1:400, Cat# A-21206, Invitrogen) or Alexa Fluor 488 donkey anti-mouse IgG (1:500, Cat# SA00013-5, Proteintech, Rosemont, IL, USA). Nuclei were stained with Hoechst 33342 (RiboBio). The negative controls were used to gate the flow plots, and then the samples were subjected to flow cytometry analysis (BD Bioscience, San Jose, CA, USA). The positive ratio of anti-let-7a-containing cells was calculated using the following formula: positive ratio = UR/(UR + LR) × 100%, where UR represented upper right and LR represented left right.

For cellular immunofluorescence analysis, the cells obtained from crushed sciatic nerves of another six rats were seeded on precoated round glass slides in a 24-well plate after the cells were filtered as described above. After 24 hours, the cells were fixed in 4% PFA, and incubated with corresponding primary specific antibodies overnight at 4°C followed by secondary antibodies for 2 hours at room temperature (the primary and secondary antibodies were the same as those listed in the "Flow cytometry analysis"). Images were taken under a fluorescence microscope (Axio Imager M2, Carl Zeiss).

Cell compatibility assay

BeaverBano™ Tissue regeneration and repair hydrogel (Cat# 30211, Beaver for Life Sciences, Suzhou, Jiangsu, China), a 1% (w/v) peptide aqueous solution with 50–200 nm aperture after gelling, was used to control release of let-7 antagomir *in vivo*, following the manufacturer's instructions.

Cell compatibility of the hydrogel was assessed using the following process. DMEM (Corning) was soaked with the hydrogel (Beaver for Life Sciences) at a ratio of 1:2 for 24 and 48 hours at 37°C. Then, the DMEM was collected and 10% FBS was added to the hydrogel-soaked culture medium. Cell survival was evaluated using a 3-(4,5-dimethyl thiazol-2-yl)-2,5-diphenyl tetrazolium bromide (MTT) assay kit (Cat# ab211091, Abcam) (Zhong et al., 2021). Purified Schwann cells were seeded at a density of 1×10^5 cells/mL per well on a 96-well plate precoated with 100 µL poly-L-lysine and containing 100 µL hydrogel-soaked culture medium (24-hour and 48-hour hydrogel-soaked groups) or DMEM with 10% FBS (control group) for 48 hours. The cells were treated with 20 µL MTT (Cat# ab211091, Abcam) reagent at a concentration of 5 mg/mL for another 4 hours at 37°C. Then the MTT reagent was carefully removed and 150 µL DMSO was added to each well to fully dissolve the formed Formazan crystals. Cell survival was measured by the absorbance at 490 nm using a microplate reader (BioTek). The data of the hydrogel-soaked group was normalized to that of the control group. Schwann cell viability was detected using a Cell Counting Kit-8 (CCK8; CK04, Dojindo Laboratories, Kumamoto, Japan). Briefly, Schwann cells were seeded at a density of 1×10^5 cells/mL per well in a well plate containing 100 µL hydrogel-soaked culture medium as described above or complete medium (control group) for 48 hours, and then treated with 10 µL CCK-8 reagent (Dojindo Laboratories) per well for another 2 hours. Cell viability was measured by the optical density value at 450 nm by a microplate reader (BioTek). The data of the hydrogel-soaked group were normalized to those of the control group.

Sciatic nerve transection and application of let-7 antagomir

let-7a antagomir (5 nmol) was dissolved in 20 µL diethyl pyrocarbonate (DEPC; R0022, Beyotime)-treated saline and mixed with 10 µL hydrogel (Beaver for Life Sciences). The mixture of let-7a antagomir and hydrogel was injected into a chitosan conduit (Nantong Xincheng Biochemical, Nantong, Jiangsu Province, China) to construct a let-7a antagomir-based chitosan-hydrogel scaffold. Thirty-six adult male rats were randomly divided into three groups and anesthetized prior to sciatic nerve transection. For the transection, 7 mm from the middle of the sciatic nerve was removed by cutting laterally with surgical scissors. In the let-7a antagomir group, the nerve gap was then bridged with let-7a antagomir. In the control group, the gap was bridged with a chitosan scaffold containing 5 nmol negative control (Con; 20 µL DEPC-treated saline and 10 µL hydrogel). Rats in the normal group received no treatment.

Immunofluorescence staining and release control assay of let-7 antagomir *in vivo*

At 4 or 8 weeks after surgery, rat sciatic nerve tissue was mounted onto microscope slides, fixed in 4% PFA, and blocked with 5% goat serum. Sections

(8 μm thickness) were incubated with mouse anti-neurofilament-200 (NF-200, neuron marker; Cat# N2912, 1:100; Sigma) overnight at 4°C followed by Alexa Fluor® 488 AffiniPure donkey anti-mouse 488 (1:500, Cat# SA00013-5; Proteintech) for 2 hours at room temperature. Dissected 30-μm sections were stained with α-bungarotoxin (1:500, Cat# B137; Sigma) for motor endplate observation, and nuclei were stained with 4′,6-diamidino-2-phenylindole (DAPI; 0100-20, SouthernBiotech, Birmingham, AL, USA). Images were taken with an Axio Imager M2 fluorescence microscope (Carl Zeiss). The number of motor endplates at different stages of maturity (plaque, intermediate, and pretzel stage) was determined, and the proportion of mature endplates was calculated as the ratio of pretzel-stage endplates out of all motor endplates (Wang et al., 2022b). For release control assay of let-7 antagomir *in vivo*, the harvested sciatic nerve segments were fixed in 4% PFA, dehydrated in 30% sucrose solution, and 12-mm-thick cryostat sections were cut at 4 weeks after surgery. Images were taken based on Cy3 Channel under a fluorescence microscope (Carl Zeiss).

Compound muscle action potential recording

At 8 weeks after surgery, rats in the control group and the anti-let-7 group were used for compound muscle action potential (CMAP) recording by using a Keypoint 2 portable electromyography system (Dantec, Copenhagen, Denmark). Recording electrodes were inserted into the mid-belly of the gastrocnemius and stimulating electrodes were inserted into the proximal and distal sciatic nerve stumps. An electric stimulus of 5 mV was delivered to evoke CMAP responses. CMAP amplitudes were recorded at both the proximal and distal nerve stumps.

CatWalk gait analysis

At 8 weeks after surgery, rats in the control and let-7a antagomir groups were subjected to CatWalk gait analysis. The CatWalk XT system (Noldus Information Technology, Wageningen, the Netherlands) with a high-speed camera that detects digital images was used to determine hind paw intensity, as previously described (Tian et al., 2018). CatWalk mean intensity was calculated using the following formula: |RH – LH|/RH, where RH indicates right hind paw mean intensity and LH indicates left hind paw intensity, to exclude inference factors. Sciatic function index (SFI) was calculated using the following formula: SFI = –38.3[(EPL – NPL) / NPL] + 109.5 [(ETS – NTS) / NTS] + 13.3[(EIT – NIT) / NIT] – 8.8, where EPL represented injured experimental site, NPL represented uninjured normal site, ETS represented toe spread, NTS represented the normal toe spread and NIT represented intermediate toe spread. An SFI value of –100 indicated loss of nerve function and an SFI value of 0 indicated normal nerve function.

Muscle weight measurement and Masson trichrome staining

At 4 and 8 weeks after surgery, the anterior tibial muscles and gastrocnemius muscles of rats in each group were collected to determine the muscle wet weight ratio. Muscles on both the injured side and the contralateral uninjured side were weighed. The wet weight ratio was calculated by dividing the wet weight of the muscle on the injured side by that of the muscle on the contralateral uninjured side. The belly of anterior tibial muscle was collected, embedded in paraffin, cut into 12-μm slices, and stained with Masson trichrome (G1340, Solarbio). Images were taken under an Axio Imager M2 microscope (Carl Zeiss).

Statistical analysis

No statistical methods were used to predetermine sample sizes; however, our sample sizes were similar to those reported in a previous publication (Lu et al., 2021). No rats or data points were excluded in a blinded assessment. Quantitative data were presented as mean ± SEM and Student's *t*-test or one-way analysis of variance followed by Dunnett's *post hoc* test were used to compare the statistical differences between groups. Statistical analysis and histograms were conducted with GraphPad Prism 6.0 (GraphPad Software, Inc., La Jolla, CA, USA). A *P*-value < 0.05 was considered significant.

Results

Endogenous expression of let-7 family in the main cell types of sciatic nerve

In sciatic nerve, Schwann cells, fibroblasts, and macrophages are the main cell types that form the regeneration microenvironment. The let-7 miRNA family contains many members, including let-7a, let-7b, let-7c, let-7d, let-7e, let-7f, and let-7i. Quantitative analysis showed that let-7a, let-7c, and let-7d were the top three highest expressed miRNAs in Schwann cells (**Figure 1A**) and fibroblasts (**Figure 1B**), and these three members were also highly expressed in macrophages (**Figure 1C**).

Regulatory relationship of let-7 family

Notably, members of the let-7 family and their negative regulator LIN28 possess a double-negative feedback loop. Changes of one member of the let-7 family may further affect other members of the let-7 family via the regulatory effect of LIN28. Considering the importance of Schwann cells in peripheral nerve repair and regeneration, Schwann cells were transfected with mimics of the top three highest expressed let-7 miRNAs: let-7a, let-7c, and let-7d. In addition to the elevation of let-7a expression, transfection with let-7a mimic elevated the expression of all other let-7 family members, especially that of let-7d, let-7e, and let-7f (**Figure 2A**). Similarly, transfection with let-7c mimic or let-7d mimic increased the expression of let-7a, let-7e, let-7f, and let-7i (**Figure 2B** and **C**). Schwann cells were then transfected with inhibitors of let-7a, let-7c, or let-7d. The let-7a, let-7c, and let-7d inhibitors reduced the expression of some let-7 family members (**Figure 2D–F**).

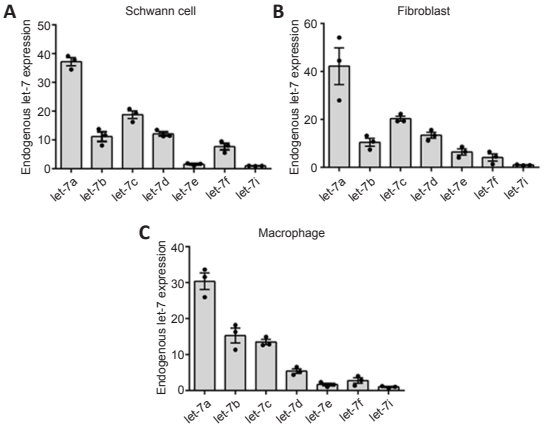

Figure 1 | **Expression levels of let-7 family members.**
Histograms showing the relative expression levels of let-7a, let-7b, let-7c, let-7d, let-7e, let-7f, and let-7i in Schwann cells (A), fibroblasts (B), and macrophages (C). Data are presented as the mean ± SEM (*n* = 3).

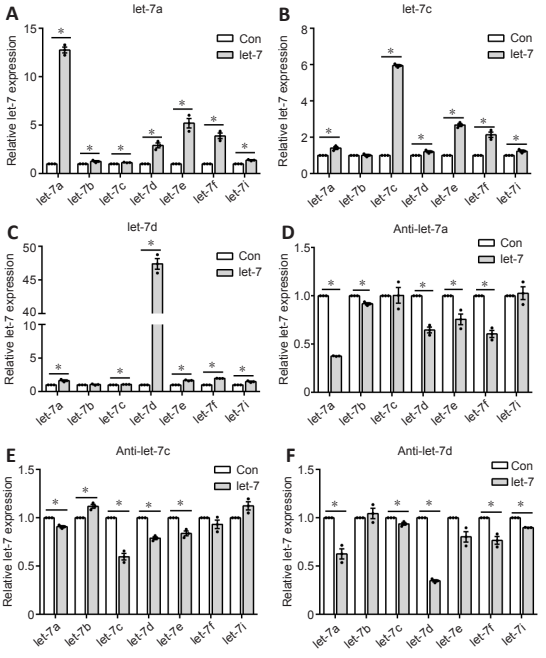

Figure 2 | **Effect of let-7a, let-7c, and let-7d on gene expression levels of other let-7 family members.**
Expression levels of let-7a, let-7b, let-7c, let-7d, let-7e, let-7f, and let-7i after the transfection of let-7a mimic (A), let-7c mimic (B), let-7d mimic (C), let-7a inhibitor (D), let-7c inhibitor (E), and let-7d inhibitor (F) in Schwann cells. Data are presented as the mean ± SEM. *P < 0.05, Student's *t*-test (*n* = 3).

Anti-let-7a is the suitable molecule for *in vivo* application from the let-7 family

Our previous study demonstrated that let-7d strongly inhibited Schwann cell proliferation and migration (Li et al., 2015b). Here, the functional effects of let-7a and let-7c were also examined. EdU cell proliferation assay showed that Schwann cells transfected with let-7a (P = 0.0110), let-7c (P = 0.0327), or let-7d (P =0.1304) mimic had significantly reduced cell proliferation rates compared with that of the control group (**Figure 3A**). In contrast, cells transfected with let-7a inhibitor (P = 0.0002), let-7c inhibitor (P = 0.0058), or let-7d inhibitor (P = 0.0030) had elevated cell proliferation rates (**Figure 3B**). Transwell-based cell migration assay showed that let-7a mimic, let-7c mimic, or let-7d mimic had an inhibitory effect on Schwann cell migration, whereas let-7a inhibitor, let-7c inhibitor, or let-7d inhibitor had a promoting effect on Schwann cell migration (**Figure 3C** and **D**). Of these results, let-7a had the most significant effects and anti-let-7a promoted the proliferation and migration of Schwann cells. Taking the results of the endogenous expression and regulatory relationship together, we considered that anti-let-7a was the most suitable molecule for *in vivo* application from the let-7 family.

The safety of let-7a antagomir (anti-let-7a)

The *in vivo* application safety of let-7a antagomir was examined by directly introducing a high dose (100 nmol) of let-7a antagomir into rats by caudal vein injection. Morphological characteristics of rat heart, liver, spleen, lung, and kidney were determined by hematoxylin-eosin staining at 5 days after let-

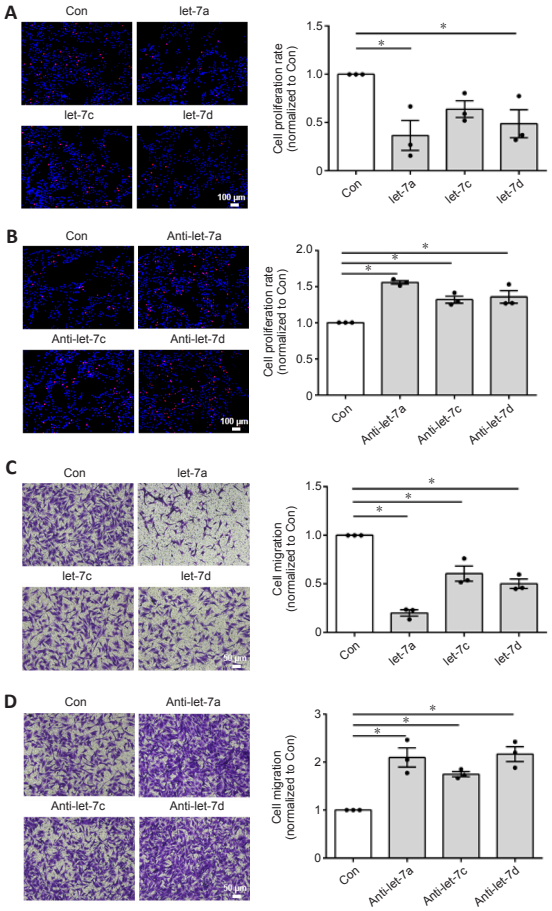

Figure 3 | **Effect of let-7a, let-7c, and let-7d on Schwann cell proliferation and migration.**
(A) Merged images of 5-ethynyl-2′-deoxyuridine (EdU) staining (red) and Hoechst 33342 staining (blue) in Schwann cells transfected with let-7a mimic (let-7a), let-7c mimic (let-7c), let-7d mimic (let-7d), and mimic control (Con). (B) Merged images of EdU staining and Hoechst 33342 staining in Schwann cells transfected with let-7a inhibitor (anti-let-7a), let-7c inhibitor (anti-let-7c), let-7d inhibitor (anti-let-7d), and inhibitor control (Con). (C) Images of migrated Schwann cells after transfection with let-7a mimic, let-7c mimic, let-7d mimic, and mimic control. (D) Images of migrated Schwann cells after transfection with let-7a inhibitor, let-7c inhibitor, let-7d inhibitor, and inhibitor control. Scale bars: 100 μm. Data are presented as the mean ± SEM. $^*P < 0.05$, one-way analysis of variance followed by Dunnett's *post hoc* test ($n = 3$).

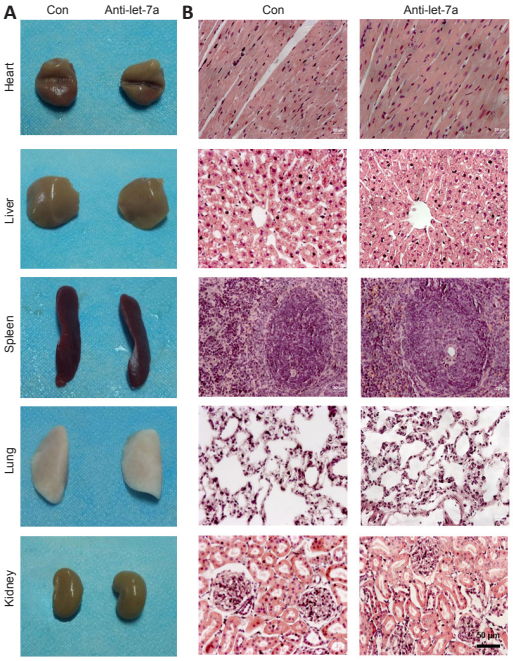

Figure 4 | **Safety assessments of rats injected with let-7a antagomir.**
(A) General observation of heart, liver, spleen, lung, and kidney in rats 5 days after injection with saline (Con) or let-7a antagomir (anti-let-7a). (B) Representative images of hematoxylin-eosin staining of heart, liver, spleen, lung, and kidney in rats injected with let-7a antagomir or saline at 5 days after injections for histopathological examinations.

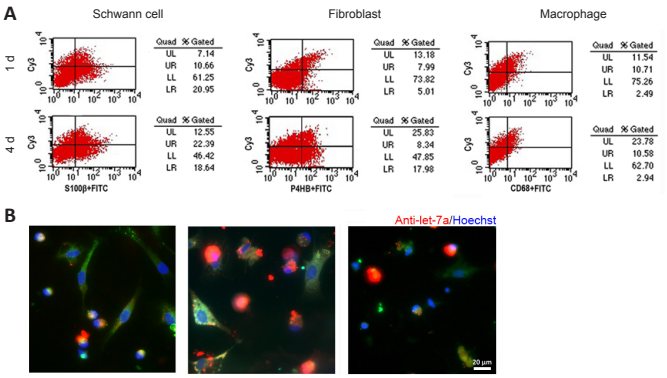

Figure 5 | **Cellular uptake of the let-7a antagomir.**
(A) Flow cytometry of Cy3-labeled let-7a antagomir in Schwann cells, fibroblasts, and macrophages at 1 and 4 days after sciatic nerve injury and let-7a antagomir injection. (B) Merged images of anti-S100β (green), anti-P4HB (green), or anti-CD68 (green) staining, Hoechst 33342 (blue), and Cy3-labeled let-7a antagomir (red) in Schwann cells, fibroblasts, and macrophages at 4 days after sciatic nerve injury ($n = 6$). Scale bar: 20 μm.

7a antagomir injection. The external appearances and weights of these organs in rats injected with let-7a antagomir were similar to those in rats injected with saline only (**Figure 4A**). Hematoxylin-eosin staining further demonstrated that the histopathological properties of these organs were not affected by let-7a antagomir injection (**Figure 4B**).

The examination of rat blood samples collected at 5 days and 4 weeks after let-7a antagomir injection showed that blood cellular and electrolyte parameters, biochemical parameters, and immunological parameters of rats treated with let-7a antagomir were not significantly different from those of saline-treated control rats (**Table 1**).

Cellular uptake of let-7a antagomir

Rat sciatic nerve injury was performed and rat sciatic nerve stumps were subjected to flow cytometry analysis to determine whether let-7a antagomir could enter into cells. At 1 day post-injury, let-7a antagomir-positive ratios in Schwann cells, fibroblasts, and macrophages were approximately 33.7%, 61.5%, and 81.1%, respectively. At 4 days post-injury, let-7a antagomir-positive ratios in Schwann cells, fibroblasts, and macrophages were approximately 54.6%, 31.7%, and 78.3%, respectively (**Figure 5A**). Immunofluorescence directly showed that let-7a antagomir entered into Schwann cells, fibroblasts, and macrophages (**Figure 5B**).

Cell compatibility assay and release control assay of hydrogel

BeaverBano™ Tissue regeneration and repair hydrogel were used to control release of let-7 antagomir *in vivo*. Good biocompatibility is essential for hydrogel application in the biomedical field. To investigate cell compatibility of the hydrogel, primary Schwann cells were cultured with complete medium (control group) or hydrogel-soaked culture medium (hydrogel-soaked group). MTT results showed that no significant difference was observed between the hydrogel-soaked culture medium and complete medium (**Figure 6A**). We further evaluated its effect on the cell viability of Schwann cells. CCK-8 assay showed no significant differences between the Schwann cells cultured in hydrogel-soaked medium and those in the control group (**Figure 6B**). Hence, the hydrogel is considered as suitable for biomedical applications.

To achieve sustained delivery of antagomir, hydrogel was used as the stabilizer and repository of let-7a antagomir. We evaluated its sustained release effect *in vivo*. The fluorescent signal of Cy3-labeled was detected at 4 weeks after the nerve grafting, suggesting that sustained release of let-7 antagomir was achieved (**Figure 6C**).

Let-7a antagomir exhibits sustained promotion of peripheral nerve regeneration

To evaluate its potential application *in vivo*, we integrated let-7a antagomir into a tissue-engineered nerve graft to bridge the gap of the sciatic nerve injury. The effect of let-7a antagomir on peripheral nerve regeneration was examined by NF-200 staining. Quantitative analysis showed that NF-200 fluorescence in the distal nerve stump in the anti-let-7 group was much lower than that in the normal group, but was significantly higher in the let-7a antagomir group compared to the normal group ($P = 0.0264$; **Figure 7A**). The morphology of motor endplates in gastrocnemius muscles observed at 8 weeks showed that in comparison with the normal group, only sparse, immature motor endplates were distributed within the target muscles of the control group (**Figure 7B**). The percentage of 'pretzel' (mature with a weblike pattern) motor endplates was much higher in the let-7a antagomir group than in the control group.

Table 1 | **Blood sample examinations of rats injected with let-7a antagomir**

	5 days			4 weeks		
Parameters	**Control**	**Anti-let-7a**	***P*-value**	**Control**	**Anti-let-7a**	***P*-value**
Blood cellular parameters						
White blood cell (× 10^9/L)	3.55±0.15	3.80±1.56	0.634	3.50±0.23	4.17±0.12	0.063
Red blood cell (× 10^{12}/L)	6.05±0.72	7.31±0.37	0.196	7.24±0.11	7.07±0.14	0.391
Platelet (× 10^{11}/L)	7.58±1.94	4.79±1.16	0.284	4.97±0.88	7.21±1.26	0.219
Hemoglobin (g/L)	125.3.0±15.25	145.3±5.68	0.307	140.7±1.20	141.7±3.53	0.802
Liver and kidney function levels and blood electrolyte parameters						
Total bilirubin (μM)	9.33±0.88	9.00±0.58	0.768	11.67±0.33	10.67±0.67	0.251
Blood urea nitrogen (mM)	6.50±0.63	6.83±0.69	0.738	6.27±0.27	7.17±0.39	0.131
Creatinine (μM)	37.33±1.20	39.67±3.33	0.546	37.33±0.88	36.00±1.53	0.492
Creatine kinase (U/L)	558.7±67.22	638.7±213.50	0.739	608.7±106.10	480.3±3.53	0.293
Glucose (mM)	9.20±0.40	8.80±0.35	0.494	11.40±0.74	11.73±0.32	0.699
Sodium (mM)	147.70±0.88	146.30±1.45	0.477	145.0±1.16	146.0±0.58	0.482
Kalium (mM)	6.93±0.23	6.00±0.06	0.018	6.63±0.18	6.27±0.09	0.137
Chlorine (mM)	100.00±0.58	97.00±1.00	0.060	96.67±1.77	98.33±0.33	0.406
Immunological markers						
Immunoglobulin G (g/L)	0.80±0.07	0.77±0.00	0.116	0.67±0.06	0.80±0.03	0.643
Immunoglobulin M (g/L)	0.20±0.06	0.20±0.03	0.962	0.23±0.01	0.19±0.02	0.128
Complement C3 (g/L)	0.27±0.03	0.23±0.03	0.519	0.30±0.00	0.27±0.03	0.374
Complement C4 (g/L)	0.030±0.006	0.027±0.003	0.643	0.027±0.007	0.027±0.003	1

Blood cellular and electrolyte parameters, biochemical parameters, and immunological parameters of rats at 5 days and 4 weeks after let-7a antagomir injection were determined and presented as the mean ± SEM.

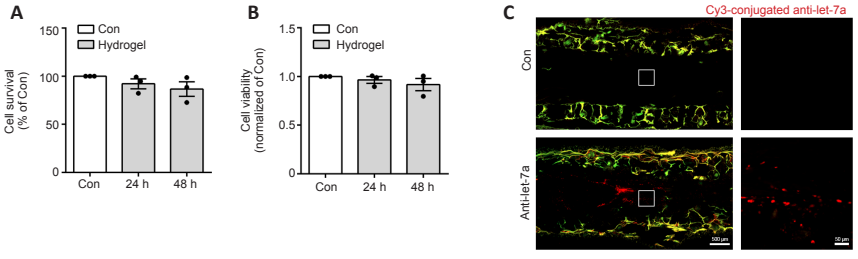

Figure 6 | **Cell compatibility and controlled release of the let-7a antagomir.**
(A) Cell compatibility was detected by the 3-(4,5-dimethyl thiazol-2-yl)-2,5-diphenyl tetrazolium bromide (MTT) assay with 100 μL mixture culture medium (24 and 48 hours Hydrogel group) or complete medium (control group, Con) for 48 hours at the absorbance of 490 nm (n = 3). (B) Cell viability was detected by Cell Counting Kit-8 (CCK8) assay in the 24 and 48 hours Hydrogel groups and control group 2 hours after CCK-8 treatment by measuring optical density at 450 nm (n = 3). (C) Fluorescence detection of Cy3-labeled let-7a antagomir at 4 weeks after surgery in nerves bridged with let-7a antagomir (anti-let-7a) or chitosan-hydrogel scaffold containing non-targeting antagomir control (Con). Boxed areas in the left images were enlarged and shown on the right. Data are presented as the mean ± SEM (n = 3).

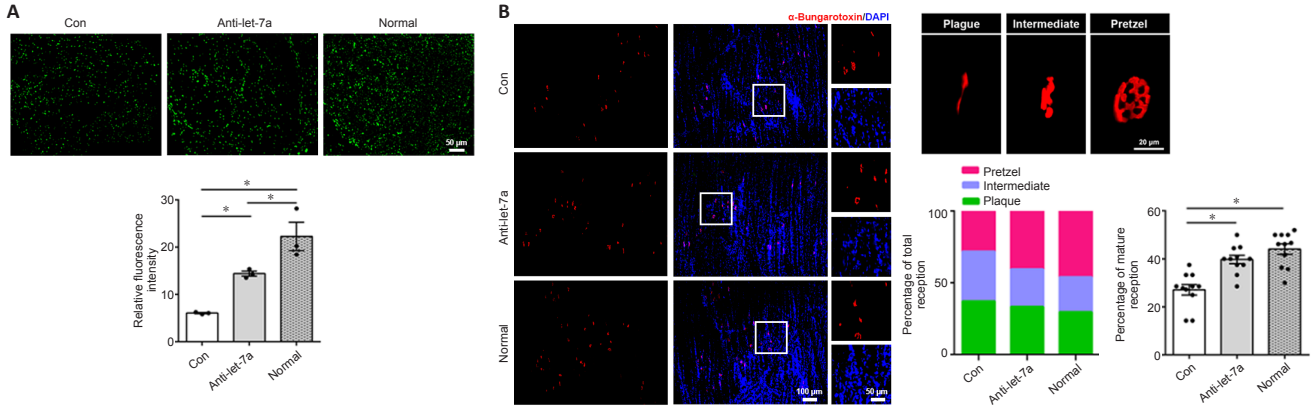

Figure 7 | **Immunohistochemistry examinations of rat sciatic nerves.**
(A) Neurofilament-200 (NF-200) staining of axons (green) in the transverse sections of normal distal nerve stumps (Normal) and distal nerve stumps bridged with let-7a antagomir (anti-let-7a) or chitosan-hydrogel scaffold containing non-targeting antagomir control (Con) 8 weeks after surgery. Scale bar: 50 μm. (B) α-Bungarotoxin (red) and 4′,6-diamidino-2-phenylindole (DAPI; blue) staining of the motor endplates at 8 weeks after surgery in transverse sections of gastrocnemius muscles (scale bar: 100 μm). The higher magnifications on the right show representative images of the motor endplates of different maturities (scale bar: 20 μm). The graph shows the maturity ratios of the motor endplates (plaque, intermediate and pretzel). Data are presented as the mean ± SEM. *P < 0.05, Student's t-test (n = 3 and 6 for A and B, respectively).

Let-7a antagomir benefits the functional recovery of injured peripheral nerves

CMAP recording showed that at 8 weeks after injury, the peak amplitudes at both the proximal site and the distal site were approximately 15 mV in the normal group. In the control group, the detected peak amplitudes were significantly lower than those in the normal group (P = 0.0002). Peak amplitudes in the anti-let-7a group were much higher than those in the control group (P = 0.0497), and reached approximately 8 mV (**Figure 8A**).

Automatic CatWalk track analysis demonstrated that injured rats showed functional improvement. The measurement of hind paw intensity showed that in let-7a antagomir-injected rats, the force and touch of the injured hind paw were closer to those of the uninjured hind paw than was observed in the control rats (P = 0.0544). At 8 weeks after injury, rats in the control group had an SFI of −88 and rats in the anti-let-7 group had an SFI value of −70, suggesting that the functional recovery of injured sciatic nerves was better in the anti-let-7 group (**Figure 8B**).

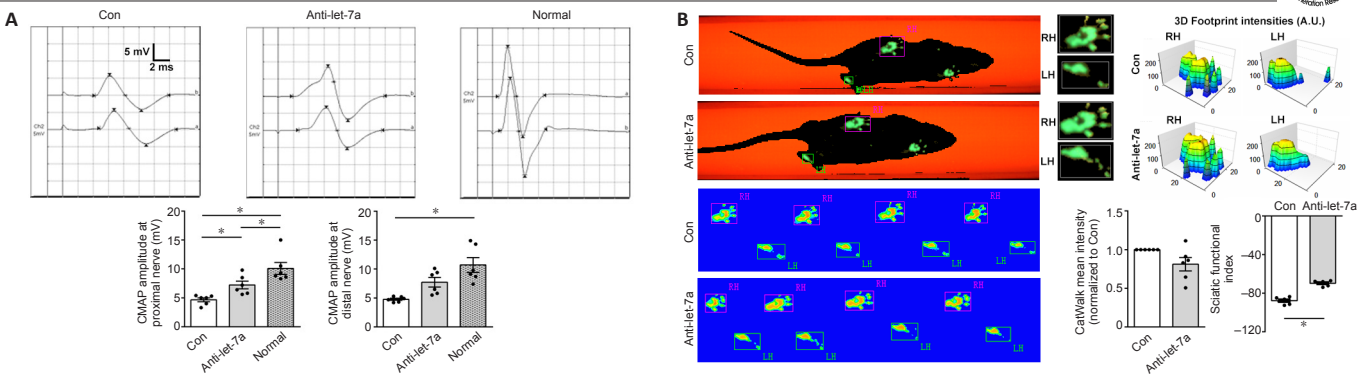

Figure 8 | **Functional examinations of rat sciatic nerves.**
(A) Compound muscle action potential (CMAP) recordings of normal rat sciatic nerves (normal) and injured nerves bridged with let-7a antagomir (anti-let-7a) or chitosan-hydrogel scaffold containing non-targeting antagomir control (Con) 8 weeks after surgery. Histograms show peak CMAP amplitudes at the proximal and the distal nerves. (B) Representative paw print images in CatWalk gait analysis and footprint intensities of rats injected with Con or let-7a antagomir (anti-let-7a) 8 weeks after surgery. CatWalk mean intensity and sciatic functional index were calculated from CatWalk recordings of the paws of injured rats. Data are presented as the mean ± SEM. *P < 0.05, Student's t-test (n = 6).

The weight and morphology of the target muscles were also measured. At 4 weeks after surgery, no differences in the wet weight ratios of the anterior tibial muscle and gastrocnemius muscle were found between the control group and the anti-let-7 group. However, at 8 weeks after surgery, the wet weight ratios of the anterior tibial muscle and gastrocnemius muscle in the anti-let-7 group were significantly higher (P < 0.0001) than those in the control group (**Figure 9A**). Observations from Masson trichrome staining showed that compared with those in the control group, muscle fibers appeared markedly larger and there were fewer collagen fibers in the anti-let-7 group at 4 and 8 weeks after surgery (**Figure 9B**).

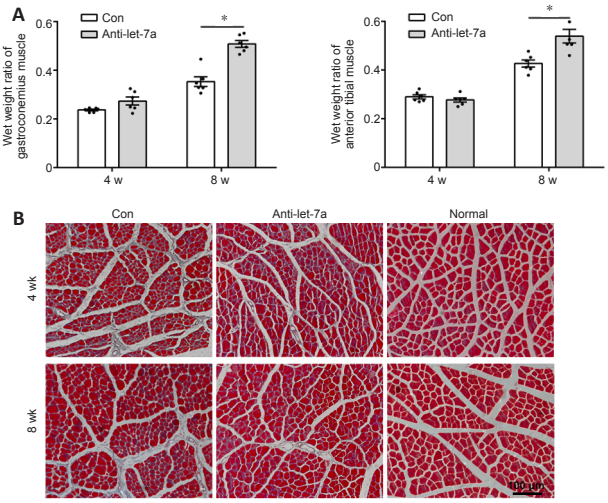

Figure 9 | **Immunohistochemistry of rat muscles.**
(A) Wet weight ratios of gastrocnemius and anterior tibialis muscles of rats bridged with let-7a antagomir (anti-let-7a) or chitosan-hydrogel scaffold containing non-targeting antagomir control (Con) at 4 and 8 weeks. (B) Masson trichrome staining of gastrocnemius muscle of normal rats (Normal) and nerve injured rats at 4 and 8 weeks after surgery. Red indicated muscle fiber staining and blue indicated collagen fiber staining. Data are presented as the mean ± SEM. *P < 0.05, Student's t-test (n = 6).

Discussion

Therapeutics targeting miRNAs have been demonstrated to have potential as treatments for genetic disorders and regenerative medicine (Beavers et al., 2015; Chew, 2015; Gori et al., 2015). Because miRNAs regulate the cellular fate of neurons and glial cells, the potential therapeutic applications of miRNAs in neural tissue engineering have gained much attention (Nguyen et al., 2015). Here, we constructed a let-7 antagomir-incorporated biomaterial to bridge peripheral nerve gaps in rats.

Quantitative analysis of let-7 family members in Schwann cells showed that let-7a, let-7c, and let-7d were expressed in relatively high levels, and that let-7a was the most abundant. Schwann cells were transfected with these highly expressed miRNAs to examine their regulatory effects on the expression of other members of the let-7 family. Transfection with let-7a mimic, let-7a inhibitor, let-7c mimic, and let-7c inhibitor significantly affected the levels of other let-7 family members. Moreover, let-7a mimic and inhibitor showed the most robust effects on Schwann cell proliferation and migration. Therefore, let-7a antagomir was used to generate the neural tissue-engineered graft.

Cellular uptake and *in vivo* stability of miRNAs are the main barriers of effective miRNA delivery (Nguyen et al., 2015). We examined the localization of let-7a antagomir by immunohistochemistry staining and found that let-7a antagomir entered into Schwann cells, fibroblasts, and macrophages. To achieve a stable and sustained release of let-7a antagomir, we dissolved let-7a antagomir in DEPC-treated saline and mixed let-7a antagomir with hydrogel in a 2:1 ratio. Hydrogel has been widely used as a delivery vehicle for short interfering RNA (Krebs et al., 2009; Perrier-Groult et al., 2013). A previous study showed that hydrogel was used to achieve controlled, localized, and sustained delivery of miRNA (Nguyen et al., 2014). Exogenous miRNA agomir or antagomir is usually steadily sustained in the body for approximately 2 weeks. Using hydrogel as the stabilizer and repository of let-7a antagomir, we found that hydrogel did not induce abnormal physiological changes and that let-7a antagomir was detectable in the injured site for at least 4 weeks after nerve injury. The mixture of let-7a antagomir and hydrogel was then injected into the chitosan conduit to effectively deliver let-7a antagomir into the injured site. Chitosan possesses favorable biocompatibility, biodegradability, and permeability. In our laboratory, chitosan-based artificial nerve grafts have been applied for peripheral nerve regeneration for a long period of time (Yang et al., 2004; Fan et al., 2008; Hu et al., 2013). Therefore, we took advantage of the properties of chitosan, and used the chitosan tube as a nerve guidance conduit to achieve the local delivery of let-7a antagomir. The joint use of hydrogel and chitosan conduit provided a useful method for the storage and sustained local release of miRNA antagomir.

The biological effect of let-7a antagomir was investigated by histological, morphological, and electrophysiological examinations. Immunohistochemistry staining, CMAP recording, CatWalk gait analysis, muscle weight measurement, and Masson trichrome staining demonstrated that let-7a antagomir significantly promoted axon elongation, increased electrophysiological response and SFI, prevented muscle atrophy, and improved nerve innervation. Histopathological, biochemical, and immunological examinations also indicated that there were no obvious adverse effects of let-7a antagomir. In summary, our study incorporated let-7a into a neural artificial nerve graft and successfully achieved sustained release of let-7a antagomir and promoted axonal growth and the reinnervation of target muscles. Our study provides an experimental basis for potential *in vivo* application of let-7 and supports clinical translational research of miRNA as a prospective alternative for regenerative medicine.

This study had several limitations. First, we did not assess long-term *in vivo* safety or later time points or perform additional nerve function assessments. Second, we evaluated cellular uptake after direct injection of the antagomir and release of the antagomir from the hydrogel in the nerve graft. However, the two methods (direct injection and hydrogel release) did not result in the exact same cellular distribution of let-7a antagomir. Third, a commercial hydrogel was used to achieve localized and sustained delivery of let-7a antagomir. In future studies, we plan to screen for a more suitable hydrogel and optimize the effect by exploring the cellular uptake and release profile of let-7a antagomir in hydrogel.

In conclusion, Let-7a antagomir is an ideal miRNA molecule to promote peripheral nerve regeneration; it has biosafety for in vivo application and it can enter into the main cell types of the sciatic nerve to optimize the regeneration microenvironment. Let-7a antagomir delivery can be effectively localized and sustained by hydrogel, and it promoted nerve regeneration and functional recovery when it was integrated into a chitosan conduit with hydrogel to construct a chitosan-hydrogel scaffold tissue-engineered nerve graft.

Author contributions: *Conceived and designed the experiments: SYL. Experiment conductance and data analyses: QQC, QYL, PW, TMQ, XHW, and SYL. Contributed reagents/materials/analysis tools: QQC and SYL. Wrote the manuscript: QQC, SY, and SYL. All authors read and approved the final manuscript.*

Conflicts of interest: *The authors declare that they have no conflict of interest that could have appeared to influence the work reported in this paper.*
Author statement: *This paper has been posted as a preprint on Research Square with doi: https://doi.org/10.21203/rs.3.rs-1100490/v1, which is available from https://assets.researchsquare.com/files/rs-1100490/v1/e78a4435-dc10-484e-830a-fea8746ed96a.pdf?c=1640105041.*
Availability of data and materials: *All data generated or analyzed during this study are included in this published article and its supplementary information files.*

Additional file:
Additional Figure 1: *Timeline of the experiment.*

References

Beavers KR, Nelson CE, Duvall CL (2015) MiRNA inhibition in tissue engineering and regenerative medicine. Adv Drug Deliver Rev 88:123-137.
Caputo M, Saif J, Rajakaruna C, Brooks M, Angelini GD, Emanueli C (2015) MicroRNAs in vascular tissue engineering and post-ischemic neovascularization. Adv Drug Deliver Rev 88:78-91.
Chen JR, Yang L, Guo L, Duan XJ (2012) Sodium hyaluronate as a drug-release system for VEGF 165 improves graft revascularization in anterior cruciate ligament reconstruction in a rabbit model. Exp Ther Med 4:430-434.
Chen RR, Mooney DJ (2003) Polymeric growth factor delivery strategies for tissue engineering. Pharm Res 20:1103-12.
Chew SY (2015) MicroRNAs in tissue engineering & regenerative medicine. Preface. Adv Drug Deliver Rev 88:1-2.
Fan W, Gu J, Hu W, Deng A, Ma Y, Liu J, Ding F, Gu X (2008) Repairing a 35-mm-long median nerve defect with a chitosan/PGA artificial nerve graft in the human: a case study. Microsurgery 28:238-242.
Gori M, Trombetta M, Santini D, Rainer A (2015) Tissue engineering and microRNAs: future perspectives in regenerative medicine. Expert Opin Biol Ther 15:1601-1622.
Gu X, Ding F, Yang Y, Liu J (2011) Construction of tissue engineered nerve grafts and their application in peripheral nerve regeneration. Prog Neurobiol 93:204-230.
Gu XS, Ding F, Williams DF (2014) Neural tissue engineering options for peripheral nerve regeneration. Biomaterials 35:6143-6156.
Hu N, Wu H, Xue CB, Gong YP, Wu J, Xiao ZQ, Yang YM, Ding F, Gu XS (2013) Long-term outcome of the repair of 50 mm long median nerve defects in rhesus monkeys with marrow mesenchymal stem cells-containing, chitosan-based tissue engineered nerve grafts. Biomaterials 34:100-111.
Hutchison ER, Kawamoto EM, Taub DD, Lal A, Abdelmohsen K, Zhang YQ, Wood WH, Lehrmann E, Camandola S, Becker KG, Gorospe M, Mattson MP (2013) Evidence for miR-181 involvement in neuroinflammatory responses of astrocytes. Glia 61:1018-1028.
Ji XM, Wang SS, Cai XD, Wang XH, Liu QY, Wang P, Cheng ZC, Qian TM (2019) Novel miRNA, miR-sc14, promotes Schwann cell proliferation and migration. Neural Regen Res 14:1651-1656.
Krebs MD, Jeon O, Alsberg E (2009) Localized and sustained delivery of silencing RNA from macroscopic biopolymer hydrogels. J Am Chem Soc 131:9204-9206.
Krutzfeldt J, Rajewsky N, Braich R, Rajeev KG, Tuschl T, Manoharan M, Stoffel M (2005) Silencing of microRNAs in vivo with 'antagomirs'. Nature 438:685-689.
Leng Q, Chen L, Lv Y (2020) RNA-based scaffolds for bone regeneration: application and mechanisms of mRNA, miRNA and siRNA. Theranostics 10:3190-3205.
Li DQ, Li X, Wang AX, Meisgen F, Pivarcsi A, Sonkoly E, Stahle M, Landen NX (2015a) MicroRNA-31 promotes skin wound healing by enhancing keratinocyte proliferation and migration. J Invest Dermatol 135:1676-1685.
Li R, Liu Z, Pan Y, Chen L, Zhang Z, Lu L (2014) Peripheral nerve injuries treatment: a systematic review. Cell Biochem Biophys 68:449-454.
Li S, Wang X, Gu Y, Chen C, Wang Y, Liu J, Hu W, Yu B, Wang Y, Ding F, Liu Y, Gu X (2015b) Let-7 microRNAs regenerate peripheral nerve regeneration by targeting nerve growth factor. Mol Ther 23:423-433.
Livak KJ, Schmittgen TD (2001) Analysis of relative gene expression data using real-time quantitative PCR and the 2(-Delta Delta C(T)) Method. Methods 25:402-408.
Lolis AM, Falsone S, Beric A (2018) Common peripheral nerve injuries in sport: diagnosis and management. Handb Clin Neurol 158:401-419.
López-Leal R, Díaz-Viraqué F, Catalán RJ, Saquel C, Enright A, Iraola G, Court FA (2020) Schwann cell reprogramming into repair cells increases miRNA-21 expression in exosomes promoting axonal growth. J Cell Sci 133:jcs239004.
Lu P, Wang G, Qian T, Cai X, Zhang P, Li M, Shen Y, Xue C, Wang H (2021) The balanced microenvironment regulated by the degradants of appropriate PLGA scaffolds and chitosan conduit promotes peripheral nerve regeneration. Mater Today Bio 12:100158.
Luo L, He Y, Jin L, Zhang Y, Guastaldi FP, Albashari AA, Hu F, Wang X, Wang L, Xiao J, Li L, Wang J, Higuchi A, Ye Q (2021) Application of bioactive hydrogels combined with dental pulp stem cells for the repair of large gap peripheral nerve injuries. Bioact Mater 6:638-654.
Miller KJ, Brown DA, Ibrahim MM, Ramchal TD, Levinson H (2015) MicroRNAs in skin tissue engineering. Adv Drug Deliver Rev 88:16-36.
Nguyen LH, Diao HJ, Chew SY (2015) MicroRNAs and their potential therapeutic applications in neural tissue engineering. Adv Drug Deliver Rev 88:53-66.
Nguyen MK, Jeon O, Krebs MD, Schapira D, Alsberg E (2014) Sustained localized presentation of RNA interfering molecules from in situ forming hydrogels to guide stem cell osteogenic differentiation. Biomaterials 35:6278-6286.
Ou L, Lan Y, Feng Z, Feng L, Yang J, Liu Y, Bian L, Tan J, Lai R, Guo R (2019) Functionalization of SF/HAP scaffold with GO-PEI-miRNA inhibitor complexes to enhance bone regeneration through activating transcription factor 4. Theranostics 9:4525-4541.
Perrier-Groult E, Pasdeloup M, Malbouyres M, Galéra P, Mallein-Gerin F (2013) Control of collagen production in mouse chondrocytes by using a combination of bone morphogenetic protein-2 and small interfering RNA targeting Col1a1 for hydrogel-based tissue-engineered cartilage. Tissue Eng Part C Methods 19:652-664.
Qian T, Wang P, Chen Q, Yi S, Liu Q, Wang H, Wang S, Geng W, Liu Z, Li S (2018) The dynamic changes of main cell types in the microenvironment of sciatic nerves following sciatic nerve injury and the influence of let-7 on their distribution. RSC Adv 8:41181-41191.
Raschzok N, Sallmon H, Pratschke J, Sauer IM (2015) MicroRNAs in liver tissue engineering- New promises for failing organs. Adv Drug Deliv Rev 88:67-77.
Roush S, Slack FJ (2008) The let-7 family of microRNAs. Trends Cell Biol 18:505-516.
Sabirzhanov B, Stoica BA, Zhao Z, Loane DJ, Wu J, Dorsey SG, Faden AI (2016) miR-711 upregulation induces neuronal cell death after traumatic brain injury. Cell Death Differ 23:654-668.
Shell S, Park SM, Radjabi AR, Schickel R, Kistner EO, Jewell DA, Feig C, Lengyel E, Peter ME (2007) Let-7 expression defines two differentiation stages of cancer. Proc Natl Acad Sci U S A 104:11400-11405.
Shen YY, Zhang RR, Liu QY, Li SY, Yi S (2022) Robust temporal changes of cellular senescence and proliferation after sciatic nerve injury. Neural Regen Res 17:1588-1595.
Su JL, Chen PS, Johansson G, Kuo ML (2012) Function and regulation of let-7 family microRNAs. Microrna 1:34-39.
Tian NX, Xu Y, Yang JY, Li L, Sun XH, Wang Y, Zhang Y (2018) KChIP3 N-terminal 31-50 fragment mediates its association with TRPV1 and alleviates inflammatory hyperalgesia in rats. J Neurosci 38:1756-1773.
Wang S, Liu X, Wang Y (2022a) Evaluation of platelet-rich plasma therapy for peripheral nerve regeneration: a critical review of literature. Front Bioeng Biotechnol 10:808248.
Wang S, Zhu C, Zhang B, Hu J, Xu J, Xue C, Bao S, Gu X, Ding F, Yang Y, Gu X, Gu Y (2022b) BMSC-derived extracellular matrix better optimizes the microenvironment to support nerve regeneration. Biomaterials 280:121251.
Wang X, Chen Q, Yi S, Liu Q, Zhang R, Wang P, Qian T, Li S (2019) The microRNAs let-7 and miR-9 down-regulate the axon-guidance genes Ntn1 and Dcc during peripheral nerve regeneration. J Biol Chem 294:3489-3500.
Wang Y, Yu T, Hu F (2022c) Hypocapnia stimuli-responsive engineered exosomes delivering miR-218 facilitate sciatic nerve regeneration. Front Bioeng Biotechnol 10:825146.
Yang YM, Gu XS, Tan RX, Hu W, Hu W, Wang XD, Zhang PY, Zhang TY (2004) Fabrication and properties of a porous chitin/chitosan conduit for nerve regeneration. Biotechnol Lett 26:1793-1797.
Yao C, Shi X, Zhang Z, Zhou S, Qian T, Wang Y, Ding F, Gu X, Yu B (2016) Hypoxia-induced upregulation of miR-132 promotes Schwann cell migration after sciatic nerve injury by targeting PRKAG3. Mol Neurobiol 53:5129-5139.
Yu B, Zhou SL, Yi S, Gu XS (2015) The regulatory roles of non-coding RNAs in nerve injury and regeneration. Prog Neurobiol 134:122-139.
Yuan J, Nguyen CK, Liu XH, Kanellopoulou C, Muljo SA (2012) Lin28b reprograms adult bone marrow hematopoietic progenitors to mediate fetal-like lymphopoiesis. Science 335:1195-1200.
Zhang JC, Zhang YQ, Chen L, Rao ZT, Sun YQ (2020) Ulinastatin promotes regeneration of peripheral nerves after sciatic nerve injury by targeting let-7 microRNAs and enhancing NGF expression. Drug Des Dev Ther 14:2695-2705.
Zhao HP, Tao Z, Wang RL, Liu P, Yan F, Li JC, Zhang CC, Ji XM, Luo YM (2014) MicroRNA-23a-3p attenuates oxidative stress injury in a mouse model of focal cerebral ischemia-reperfusion. Brain Res 1592:65-72.
Zhong B, Guo S, Yang Z, Han L, Du J, Chen J, Dun X, Wang G (2021) Roflumilast reduced the IL-18-induced inflammatory response in fibroblast-like synoviocytes (FLS). ACS Omega 6:2149-2155.

C-Editor: Zhao M; S-Editor: Li CH; L-Editors: McCollum L, Li CH, Song LP; T-Editor: Jia Y

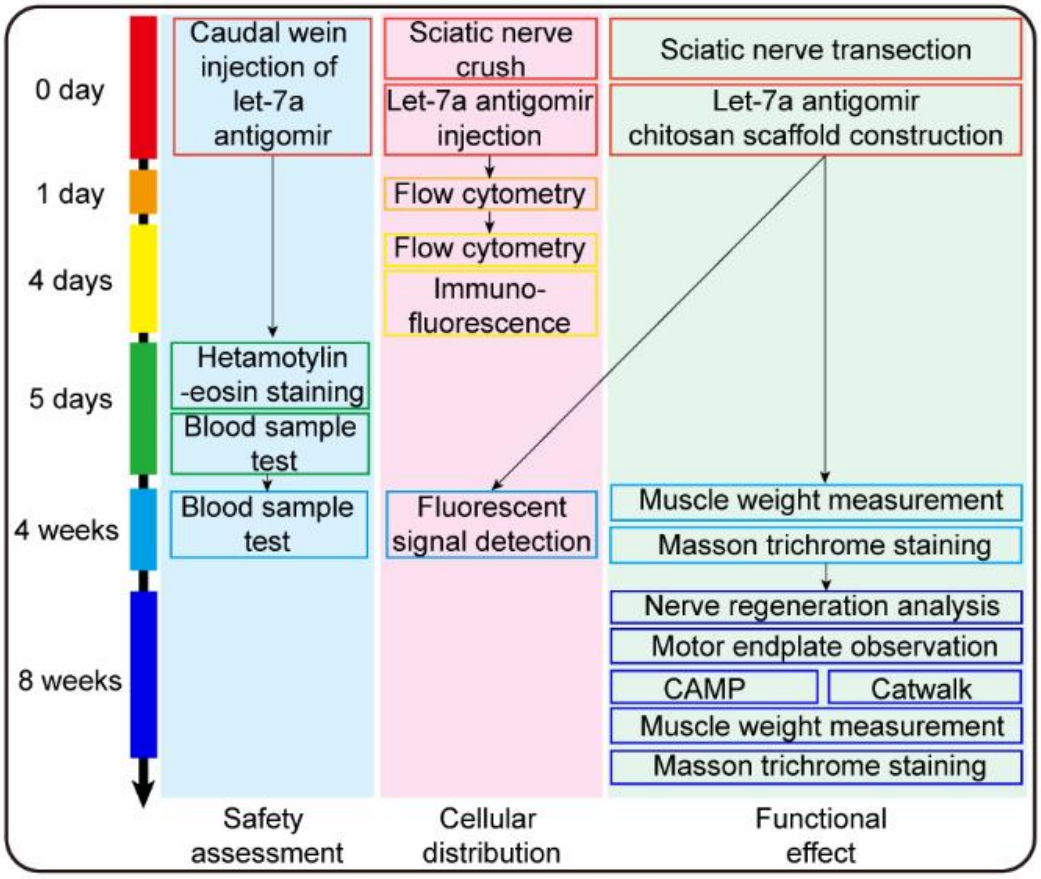

Additional Figure 1 Timeline of the experiment.